Failure phenomena in two-dimensional multi-fibre microcomposites, Part 2: A Raman spectroscopic study into the influence of inter-fibre spacing on stress concentrations

ELSEVIER

PII: S0266-3538(97)00004-3

Composites Science and Technology **57** (1997) 899–911

0266-3538/97/$17.00

FAILURE PHENOMENA IN TWO-DIMENSIONAL MULTI-FIBRE MICROCOMPOSITES: 2. A RAMAN SPECTROSCOPIC STUDY OF THE INFLUENCE OF INTER-FIBRE SPACING ON STRESS CONCENTRATIONS

P. W. J. van den Heuvel,[a,b] T. Peijs[a] & R. J. Young[b]*

[a]*Centre for Polymers and Composites, Eindhoven University of Technology, PO Box 513, 5600 MB Eindhoven, The Netherlands*

[b]*Manchester Materials Science Centre, UMIST/University of Manchester, Grosvenor Street, Manchester M1 7HS, UK*

(Received 6 June 1996; revised 4 November 1996; accepted 26 November 1996)

Abstract

Raman spectroscopy is used to determine the influence of inter-fibre spacing on the stress concentration factor (SCF) resulting from a fibre break in a two-dimensional (2-D) carbon/epoxy microcomposite. Microcomposites with an inter-fibre spacing varying from 0·8–19·0 fibre diameters (ϕ) have been investigated. The SCF was found to decrease from a value of 1·26 at an inter-fibre spacing of 0·8ϕ to a value of 1·06 at an inter-fibre spacing of 10·4ϕ. The experimentally found variation of SCF with inter-fibre spacing was compared to some analytical models available in the literature. It was found that none of the models is able to describe the experimental data adequately. The effect of the SCF on the failure process is also discussed. At relatively small inter-fibre spacings the SCF is sufficiently high to cause further fibre failure in neighbouring fibres resulting in alignment of fibre breaks. At increasing inter-fibre spacing the decrease in SCF results in a decreasing influence of the initial fibre break on the progressive fibre failure process and the failure process becomes more random. © 1997 Elsevier Science Limited

Keywords: Raman spectroscopy, stress concentrations, composites, carbon fibre, carbon/epoxy

1 INTRODUCTION

Failure in fibre-reinforced materials is a complex mixture of microscopic events such as fibre failure, matrix cracking and fibre/matrix debonding, each of which influences the stress state in the composite and, hence, the failure process. In order to come to an understanding of composite strength, for example, a knowledge of each of these microscopic events is necessary. However, this still proves to be a difficult task as a result of the complexity of the problem. For instance, carbon fibre exhibits considerable variability in tensile strength with its length, attributed to flaws whose position and intensity vary along the fibre length.[1–3] As a result, on loading a composite fibre, fractures are observed at tensile stresses well below the fracture stress of the composite. As the load increases, fibre fractures accumulate until the composite can no longer sustain the load and macroscopic failure of the composite takes place. In the failure process, some fibres fail as a result of the actual load applied to the composite, others fail as a result of the overload surrounding already broken fibres. This overload in the area surrounding a fibre break is due to the fact that a broken fibre does not take full loading along a certain length from the break, i.e. the ineffective length, and hence excess load is distributed over the area surrounding the break. Because of the large difference in stiffness between the fibres and the matrix, most of this overload is carried by the fibres resulting in stress concentrations in the fibres. The length over which the fibre is overloaded is called the positively affected length (see Fig. 1).

The effect of overload on strength was analyzed in a classic study by Daniels.[4] In this study he considered a loose fibre bundle, i.e. without any matrix present, and he assumed that the overload was shared equally by all intact fibres (equal load sharing). The equal load sharing theory of Daniels for loose bundles was used by Rosen[5] to predict the uni-axial strength of fibre-reinforced composites. However, for fibre-reinforced composites equal load sharing lacks realism. Since, in a fibre-reinforced composite, the immediate lateral neighbours to a broken fibre bear most of the excess load, whereas the more distant fibres carry only a small fraction of the overload and

* To whom correspondence should be addressed.

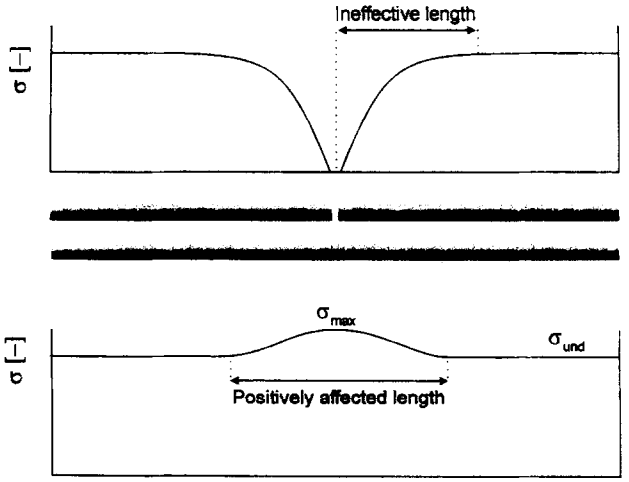

Fig. 1. Schematic illustration of the stress build-up in a broken fibre and in an adjacent fibre, showing the ineffective length and the positively affected length.

fibres sufficiently far away from the fibre break do not even detect the break, i.e. they do not carry the overload at all. Indeed, one usually observes clusters of breaks throughout the whole of the composite.[5,6] Evidently, local load sharing occurs and the magnitude of the overload at both a certain lateral and longitudinal distance from a fibre break depends on the mechanical properties of the fibre and the matrix, the fibre/matrix interface and the inter-fibre spacing.[7] To describe conveniently the overloading of an intact fibre as a result of a broken fibre, a stress concentration factor (SCF), K, is defined as the ratio between the maximum stress in the intact fibre and the stress in the undisturbed part of the intact fibre, i.e. far away from the break (see Fig. 1):

$$K = \frac{\sigma_{\max}}{\sigma_{\text{undisturbed}}} \tag{1}$$

Hedgepeth and Van Dyke[8] were among the first to calculate the stress concentration factor in a planar array of fibres. Using a shear-lag approach in which the fibres carry only axial loads and the matrix carries only shear loads developed earlier by Cox[9] they derived the following expression for the SCF in an intact fibre due to q adjacent fibre breaks:

$$K_q = \prod_{j=1}^{q} \frac{2j+2}{2j+1} \tag{2}$$

From eqn (2) it is seen that in case of one fibre break ($q = 1$) the SCF is 1·33. Using the local load sharing assumption, Harlow and Phoenix[7] proposed the following SCF for a circular array of evenly spaced fibres:

$$K_q = 1 + \frac{q}{2} \tag{3}$$

where q now is the number of broken fibres immediately adjacent to an unbroken fibre. In both these local load sharing theories, however, the SCF is independent of the mechanical properties of the fibre and the matrix, the fibre/matrix interface, and the fibre volume fraction, i.e. inter-fibre spacing. Aware of this deficiency, Fukuda and Kawata[10] were the first to incorporate the material properties of the fibre and the matrix, in terms of the fibre modulus, E_f, the matrix modulus, E_m, and the fibre volume fraction, V_f, into the calculation of the SCF. In contrast to Hedgepeth and Van Dyke,[8] Fukuda and Kawata[10] assumed that the matrix carries not only shear stresses but also axial stresses. Their analysis showed that the SCF increases with increasing value of the ratio E_f/E_m, with decreasing inter-fibre spacing, and with increasing number of adjacent broken fibres, q. A further improvement was made by Ochiai and coworkers[11–13] by incorporating the influence of matrix cracking and fibre/matrix debonding on the SCF in their shear-lag analysis. They found that matrix cracking increases the SCF and that debonding decreases the SCF. A totally different approach was followed by Bader and coworkers[14,15] and Wolstenholme.[6] The following was proposed for the maximum SCF as a function of q:

$$K_q = 1 + \frac{\sqrt{q}}{f} \tag{4}$$

where f is a load-sharing parameter.[14] In order to obtain a value for K, the load-sharing parameter has to be known. By using a maximum likelihood procedure, Wolstenholme[6] calculated this load-sharing parameter at various inter-fibre spacings using tungsten-cored silicon carbide fibres embedded in epoxy resin, developed earlier by Clarke and Bader.[15] More recently, following the 'zone of influence' concept introduced by Cherepanov,[16] Wagner and Eitan[17] developed a new theory to calculate the SCF. In this theory, they defined an effective radius around the fibre break in which the overload is transferred to the intact adjacent fibres. By using conventional shear-lag theory (the matrix carries shear stress only and perfect fibre/matrix bonding exists) the following expression was derived for the influence of the inter-fibre spacing, d_i, and fibre radius, r_f, on the SCF:

$$K = 1 + \frac{1}{\Pi}\sin^{-1}\left(\frac{r_f}{d_i}\right) \tag{5}$$

The model of Wagner and Eitan was slightly modified by Grubb *et al.*[18] Where Wagner and Eitan[17] use the fibre radius, r_f, to determine the limits of the load transfer area, Grubb *et al.*[18] use the experimentally-determined fibre/fibre interaction radius, r_e:

$$K = 1 + \frac{1}{\Pi}\cos^{-1}\left(\frac{d_i}{2r_e}\right) \tag{6}$$

As seen from eqns (5) and (6) both theories predict a decrease in SCF with increasing inter-fibre spacing.

The SCFs predicted by Eitan and Wagner are, however, lower than the values calculated by Grubb *et al.*

Evidently, there is a variety of theories all predicting different SCFs. Until recently it was not possible to verify these theories with experimental data. However, current developments in Raman spectroscopy allow for the *in situ* mapping of local strains in a fibre and, hence, the determination of stress concentrations in real composites has now become possible.[18–23] In a recent study Grubb *et al.*[18] were able to measure the presence of stress concentrations in Nicalon/Kevlar and carbon/Kevlar 2-D hybrid microcomposites. A hybrid structure is useful to induce a fibre break (Nicalon and carbon both have a lower strain to failure than Kevlar) but limit the investigation to measurement of the SCF only. The failure process in the microcomposite that results from the SCF cannot be properly related to the failure process in a real carbon/epoxy composite. In a recent study Wagner *et al.*[22] an attempt was made to measure SCFs in a 2-D microcomposite containing Kevlar 149 fibres only. However, they failed to properly measure SCFs as a result of the splitting failure mode of the fibres used. In contrast, using a 2-D microcomposite containing carbon fibres Van den Heuvel *et al.*[23] were able to measure the stress concentrations at two inter-fibre spacings. At inter-fibre spacings of 0·8 and 2·0, SCFs of 1·26 and 1·19 were found, respectively. In the present paper of this series of papers concerning failure phenomena in multi-fibre microcomposites,[23–25] we present a quantitative investigation into the influence of inter-fibre spacing on the actual stress concentrations using the Raman technique. Furthermore, the experimental results will be compared to some of the aforementioned theories on stress concentrations in intact fibres resulting from broken fibres.

2 EXPERIMENTAL

2.1 Materials

The fibres used in this study were high-modulus polyacrylonitrile (PAN) based, surface-treated Tenax HMS-40 (Akzo Tenax Fibers GmbH and Co. KG) carbon fibres ($E_f = 350$ GPa). Initially, an epoxy size was present on the fibres. Drzal *et al.*[26] have shown that such a sizing influences the failure mode of the microcomposite. In the context of our research project into failure processes in microcomposites we want to exclude this influence of the size and, hence, the size was removed. The fibres were washed twice in acetone for several hours.[20] Weighing of the unsized fibres confirmed removal of the size. The average fibre diameter, ϕ, was reported by Gu *et al.*[20] and measured $6{\cdot}73 \pm 0{\cdot}21$ μm. The matrix used consisted of a common diglycidyl ether of bisphenol A (DGEBA) type epoxy (Ciba Geigy, Araldite LY556) and a stoichiometric amount of poly(oxypropylene)tri-amine (Texaco, Jeffamine T-403) curing agent. Preparation of the multi-fibre microcomposites is described in detail elsewhere.[25] The resin mixture was cured at room temperature for 24 h and post-cured at 75°C for 16 h. Tensile tests performed on a universal tensile tester (Frank 81565) provided the Young's modulus ($E_m = 2{\cdot}7$ GPa) of the matrix. The shear yield stress of the matrix was determined with a simple shear-test setup (ASTM, 04255-83) giving 37 MPa at a shear strain rate of 10^{-3} s^{-1}.

2.2 Raman spectroscopy

The variation of the Raman signal of the carbon fibre with strain was determined by deformation of the carbon fibres in air. Single fibres were mounted in a straining rig with a cardboard frame, as in the procedure described in ASTM D-3379. To reduce the influence of end effects a relatively long gauge length of 100 mm was chosen. The deformation direction of the fibre was within ±5° of the fibre axis and the displacement of the fibre was determined to an accuracy of ±5 μm using a micrometer attached to the straining rig. In this way, the strain in the fibres could be measured to an accuracy of about 0·01%. Raman spectra were obtained using a Raman spectrometer system (Renishaw 1000) coupled to an optical microscope (Olympus BH-2). The spectra were obtained using the 632·8 nm red line of a 25 mW helium–neon laser (Spectra Physics Model 127-25). Using a ×50 objective lens a laser-beam spot of approximately 2 μm was focused on the fibre surface which gave a laser beam intensity of <2·5 mW at the sample.

For analysis of the multi-fibre microcomposite, the microcomposite was strained in a miniature tensile tester (Minimat, Polymer Laboratories) equipped with a 1000 N load cell using manual control. The strain on the microcomposite was monitored and controlled accurately using a strain gauge mounted directly on the specimen.

3 RESULTS

3.1 Raman deformation of Tenax HMS-40

Extended spectra of a Tenax HMS-40 fibre in air and embedded in the epoxy are presented in Fig. 2. It can be seen that Tenax HMS-40 has three Raman peaks located at 1330, 1580 and 2660 cm^{-1} and that the epoxy shows substantial Raman activity in the range 500–1700 cm^{-1}. Because of the large Raman activity of the epoxy in the lower wavenumber region, the 2660 cm^{-1} Raman peak of the carbon fibre is chosen for mapping the strain along the fibres. Figure 3 shows the 2660 cm^{-1} Raman band for a fibre in air in the unstrained state and at a tensile strain of 0·75%. As commonly observed, the increase in tensile strain results in a clear shift of the peak to a lower

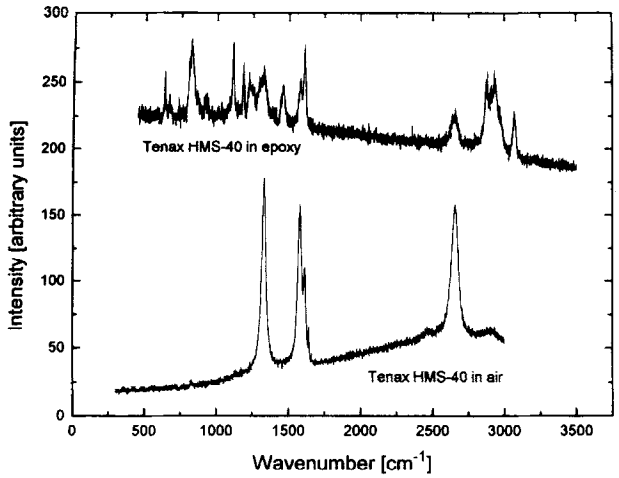

Fig. 2. Extended Raman spectrum of a Tenax HMS-40 carbon fibre in air superimposed on the Raman spectrum of the fibre embedded in the epoxy microcomposite.

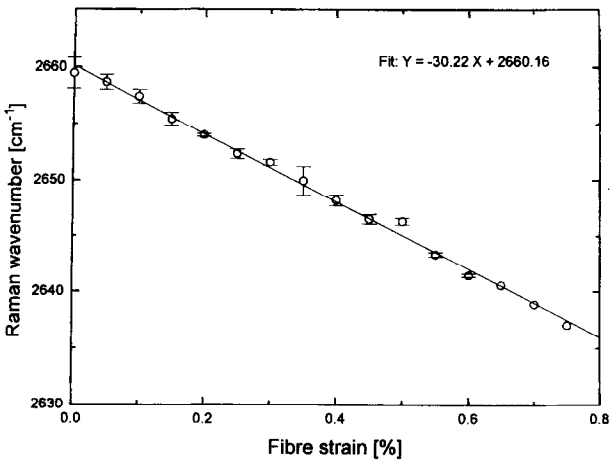

Fig. 4. Strain/wavenumber calibration curve for Tenax HMS-40 carbon fibre. The error bars indicate the standard deviation of the mean value of four fibres.

wavenumber.[18–23] In order to determine the positions of the Raman peaks a Lorentzian fitting procedure was used. The variation of the peak position of the 2660 cm^{-1} Raman band with strain was determined for four Tenax HMS-40 fibres and is shown in Fig. 4. An approximately linear decrease of Raman peak position with strain was found. It can also be seen that the error in the measurement of the position of the 2660 cm^{-1} Raman band is of the order of ± 1 cm^{-1}. The sensitivity of the 2660 cm^{-1} Raman peak towards an increase in strain was found to be $-30{\cdot}2$ cm^{-1}/%. This means that in the microcomposites the strain can be measured to an accuracy of approximately 0·03%.

3.2 Raman observations of the failure process

Microcomposites with inter-fibre spacings varying from $0{\cdot}8\phi$ to $19{\cdot}0\phi$ were produced and the strain profiles along a length of 2000–2500 μm of each of the five fibres in the microcomposite were measured at increasing strain levels. Figure 5(a) shows the strain profiles of each of the five fibres at a relatively small inter-fibre spacing at a matrix strain of 0%. Measurements were taken at 50 μm intervals. In Fig. 5(b) the macroscopic strain of the specimen has been increased to 0·9%. Raman spectra were taken at 10 μm intervals in the vicinity of the break, at 20 μm intervals further away from the break, and at 50 μm intervals far away from the break. At $x = 0$ μm a break can be clearly observed in the centre fibre (Fibre 3) resulting in increased strains in its adjacent fibres (Fibres 2 and 4). Unfortunately, due to the scatter in the strain in Fibres 1 and 5 no information about possible shielding of the stress by Fibres 2 and 4 can be obtained. Figure 5(c) shows the strain profiles of each fibre at a matrix strain of 1·1% when further fragmentation has occurred. Alignment of breaks as a result of the increased strains around the initial fibre break is clearly observed for all fibres. In Fig. 5(d) the matrix strain is increased to approximately 1·7%. Microscopical observations showed that no more breaks were formed, i.e. the saturation stage was reached. It can be seen that all of the fibre fragments have maximum strains far below the applied strain, confirming saturation of the fragmentation process.

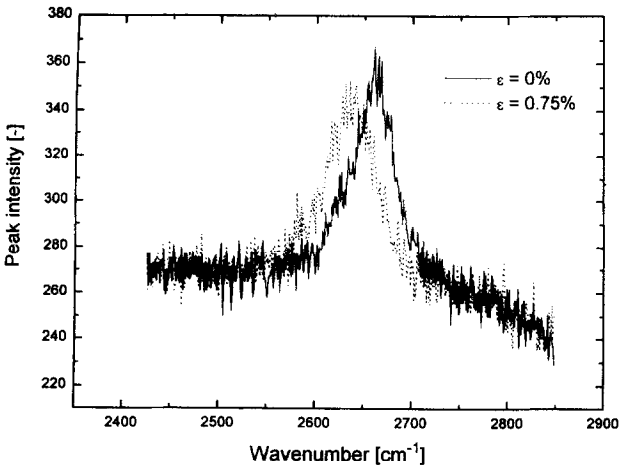

Fig. 3. Raman spectra of Tenax HMS-40 carbon fibre in air showing the shift of the 2660 cm^{-1} Raman band with increasing strain.

Figure 6 shows strain profile plots for each fibre in the microcomposite at increasing strain for intermediate inter-fibre spacing. Similar observations as for the small inter-fibre spacing in Fig. 5 are made with aligned fibre breaks. However, in this particular specimen the saturation stage of the fragmentation process could not be reached due to premature macroscopic failure of the model composite. Figure 7 shows the strain profiles for a microcomposite in which the inter-fibre spacings are relatively large. It

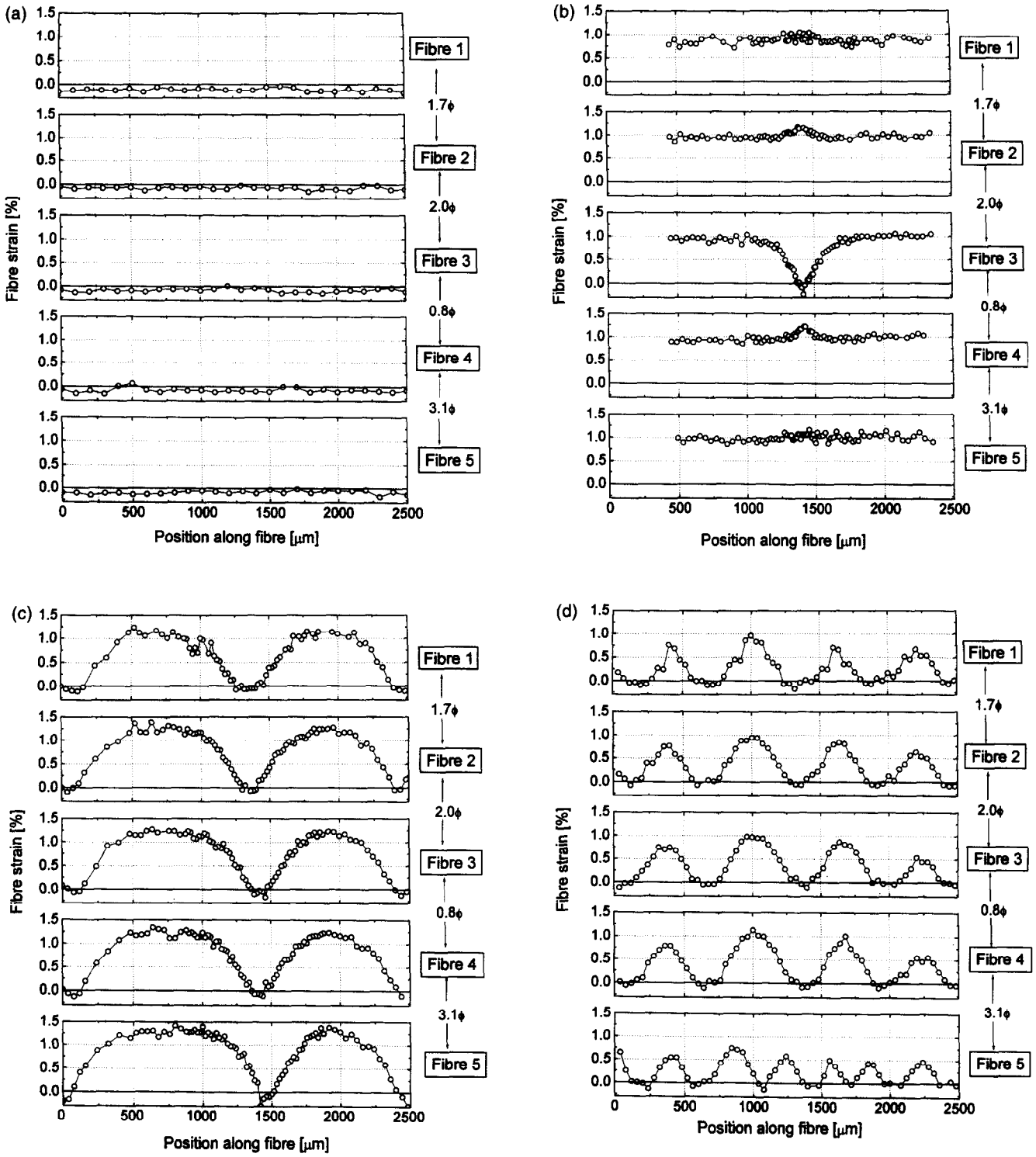

Fig. 5. Strain profiles determined from stress-induced Raman band shifts for a Tenax HMS-40/epoxy microcomposite containing a 2-D array of five fibres with a relatively small inter-fibre spacing. The inter-fibre spacing is indicated in each plot in terms of the fibre diameter, ϕ. The applied strain is (a) 0%, (b) 0·9%, (c) 1·1%, (d) 1·7%.

was found that at the inter-fibre spacing of $10{\cdot}4\phi$ in between Fibres 4 and 5 the SCF is still significantly present (Fig. 7(b)). However, at the slightly higher inter-fibre spacing of $12{\cdot}2\phi$ in between Fibres 3 and 4 the SCF is difficult to resolve within the scatter.

3.3 Fitting procedures

In order to obtain information about the SCF and the shear stresses acting upon the fibres the experimental data were fitted using the following procedure. The strain profile, ε_f, of each end of the broken fibre was

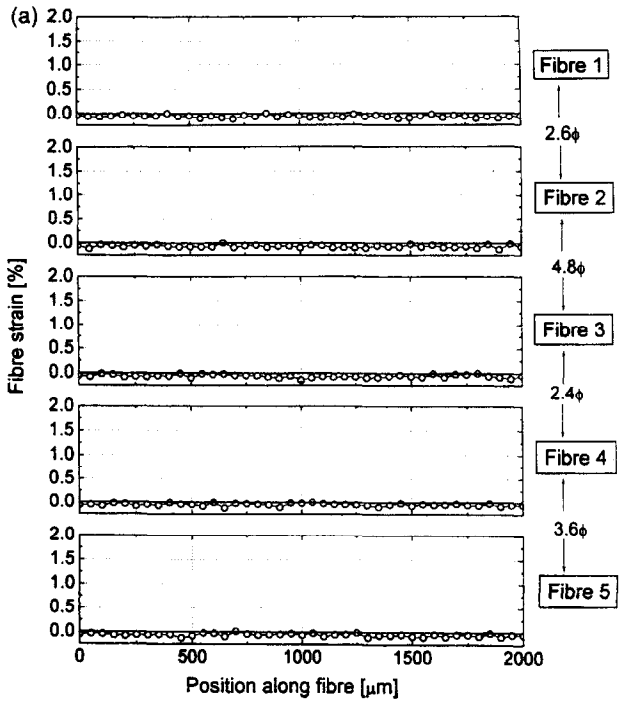

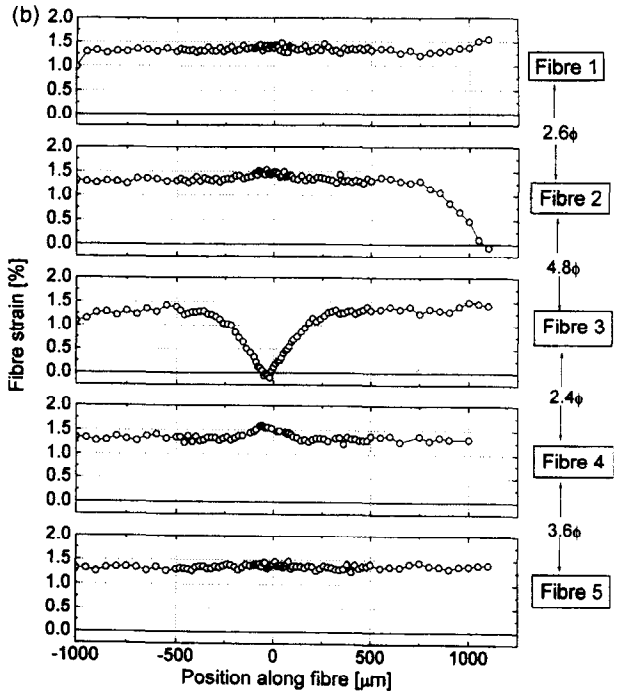

Fig. 6. Strain profiles determined from stress-induced Raman band shifts for a Tenax HMS-40/epoxy micro-composite containing a 2-D array of five fibres with an intermediate inter-fibre spacing. The inter-fibre spacing is indicated in each plot in terms of the fibre diameter, ϕ. The applied strain is (a) 0%, (b) 1·3%, (c) 1·5%.

fitted to a Piggott model,[27] i.e. immediately behind the fibre break linear stress build-up takes place followed by elastic stress build-up according to Cox's shear-lag theory.[9,28] The following equation was used to fit the

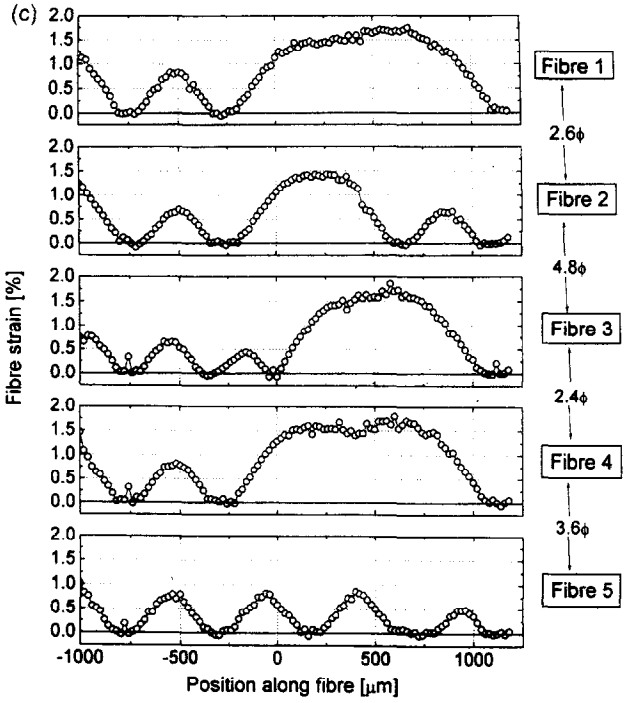

Fig. 6. (*Continued.*)

strain profile in each fibre end:

$$\varepsilon_f = \frac{2\tau_y}{rE_f}|x - x_0|, \quad |x_0| < |x| < |x_y|$$

$$\varepsilon_f = \frac{2\tau_y}{rE_f}|x_0 - x_y| + \left(\varepsilon_m - \frac{2\tau_y}{rE_f}|x_0 - x_y|\right) \times \left(1 - \frac{\cosh(\beta(0{\cdot}5l - |x_y - x|))}{\cosh(\beta 0{\cdot}5l)}\right), \quad |x| > |x_y| \tag{7}$$

where τ_y represents the shear stress at the fibre/matrix interface in the linear stress build-up region, r is the fibre radius, x is the position along the fibre, x_0 is the position of the fibre break, x_y is the end of the linear region, l is the length over which elastic stress build-up is taking place, and β is given by:

$$\beta = \frac{1}{r}\left[\frac{E_m}{(1+\nu_m)E_f \ln(r_m/r)}\right]^{1/2} \tag{8}$$

where ν_m is the Poisson ratio of the matrix and r_m is the radial distance from the fibre axis at which the matrix strain is unaffected by the presence of the fibre. In order to obtain the maximum SCF from the experimental data, the strain profiles of the SCF in the fibres adjacent to a broken fibre were fitted with a Gaussian distribution function. Using the balance of forces across an infinitesimal fibre fragment the interfacial shear stress (ISS) acting upon the fibre was simply calculated from:[10,19]

$$\tau = E_f \frac{r}{2}\left(\frac{d\varepsilon}{dx}\right) \tag{9}$$

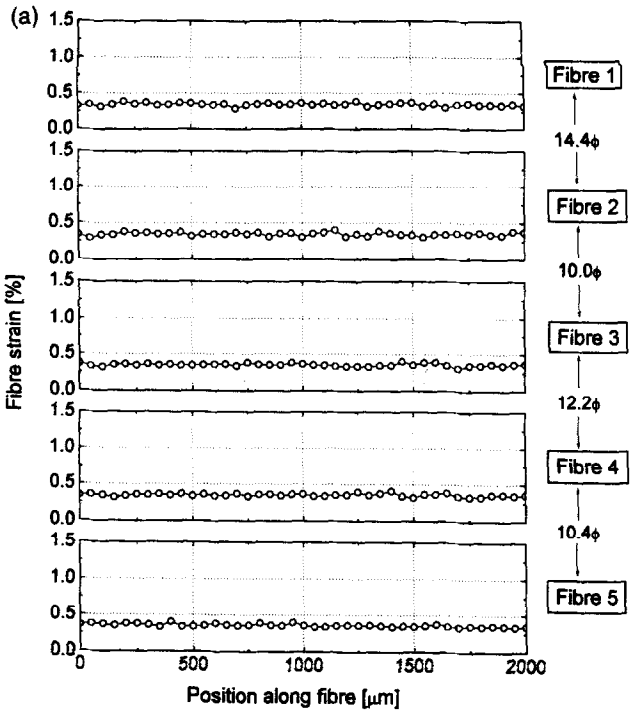

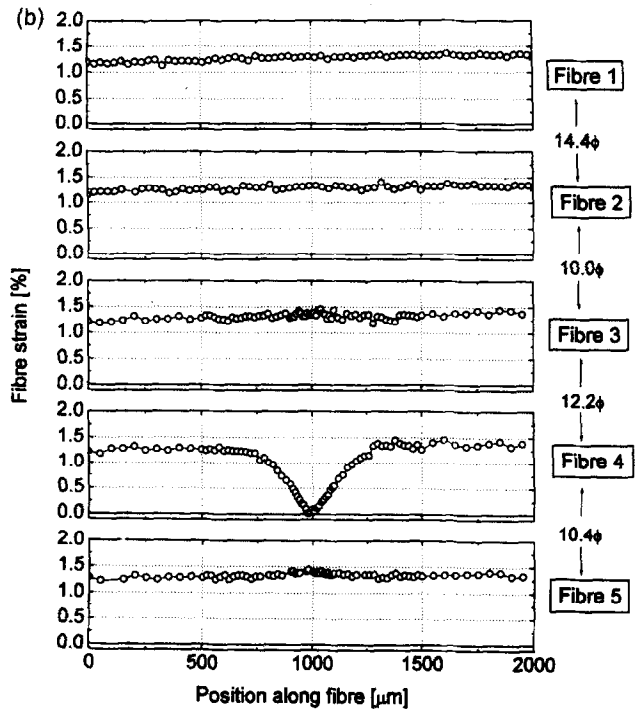

Fig. 7. Strain profiles determined from stress-induced Raman band shifts for a Tenax HMS-40/epoxy microcomposite containing a 2-D array of five fibres with a relatively large inter-fibre spacing. The inter-fibre spacing is indicated in each plot in terms of the fibre diameter, ϕ. The applied strain is (a) 0%, (b) 1·3%, (c) >1·3% (strain gauge detached).

Results of the fitting procedure for a small, an intermediate and a large inter-fibre spacing are presented in Fig. 8. Figure 8(a) shows the results of the fitting procedure for Fibres 3 and 4 of Fig. 5

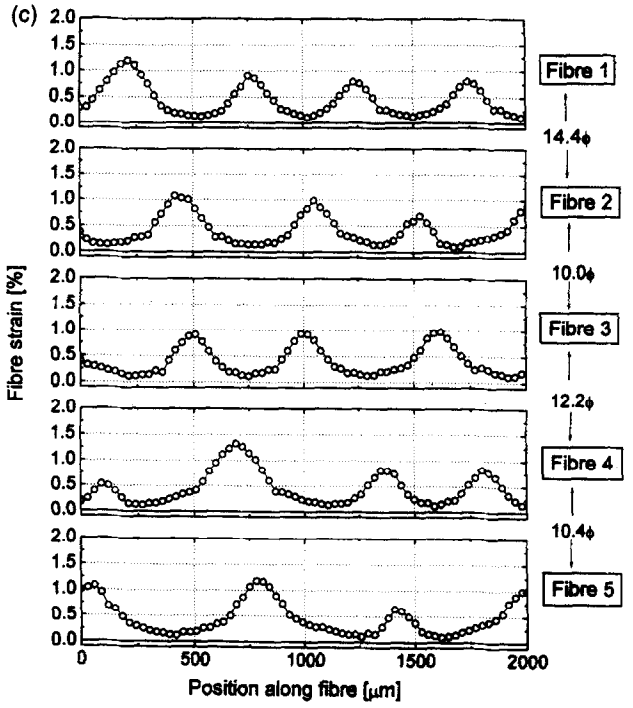

Fig. 7. (*Continued.*)

(inter-fibre spacing of 0·8ϕ), Fig. 8(b) shows the results of Fibres 3 and 4 (inter-fibre spacing of 2·4ϕ), and Fig. 8(c) shows the results for Fibres 4 and 5 of Fig. 7 (inter-fibre spacing of 10·4ϕ). In the fitting procedure for the stress build-up around a fibre break $E_f = 350$ GPa, $E_m = 2{\cdot}7$ GPa, $r = 3{\cdot}36$ μm, and for ν_m a value 0·41 was assumed. It can be seen that both the fibre break and the SCF are fitted well by the equations. In order to fit the elastic part of the strain profiles r_m was given a value of 25r. This is of a similar order to that of Galiotis,[29] who reported a value for r_m of 10–15 for a Kevlar/epoxy single-fibre microcomposite.

In addition, an attempt was made to fit the strain profiles of the fibre fragments in the saturated stage using eqn (7). However, eqn (7) was found not able to fit the strain profiles adequately because the elastic part of eqn (7) could not be fitted to the data (see Fig. 9(a)). A Piggott type stress transfer model[27] consisting of two (Kelly–Tyson[30]) linear stress build-up regions, one for debonding and the other for yielding, was found to fit the experimental strain profiles better:

$$\varepsilon_f = \frac{2\tau_i}{rE_f}|x - x_0|, \quad |x_0| < |x| < |x_d|$$
$$\varepsilon_f = \frac{2\tau_d}{rE_f}|x_d - x_0| + \frac{2\tau_y}{rE_f}|x - x_d|, \quad |x| > |x_d| \tag{10}$$

where x_d represents the end of the debonded zone and τ_i is the (frictional) shear stress in the debonded area. Figure 9 shows the results of the fitting procedure using eqn (10) for saturated fibres in the case of small, intermediate, and large inter-fibre spacings. The

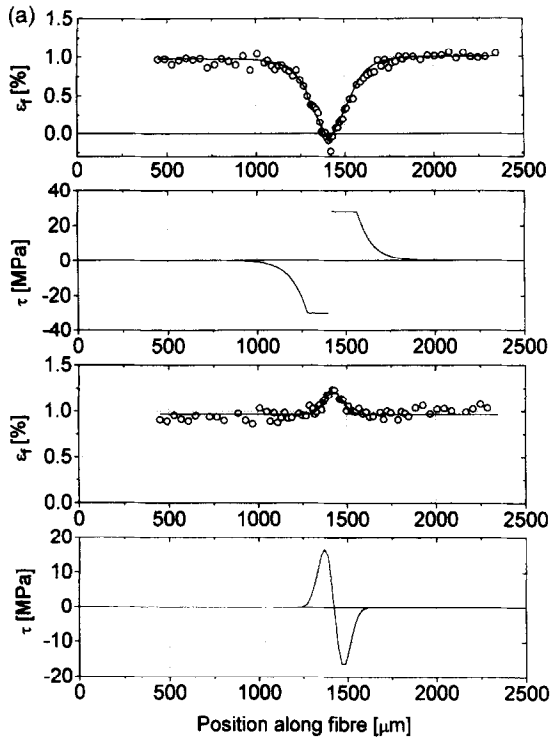

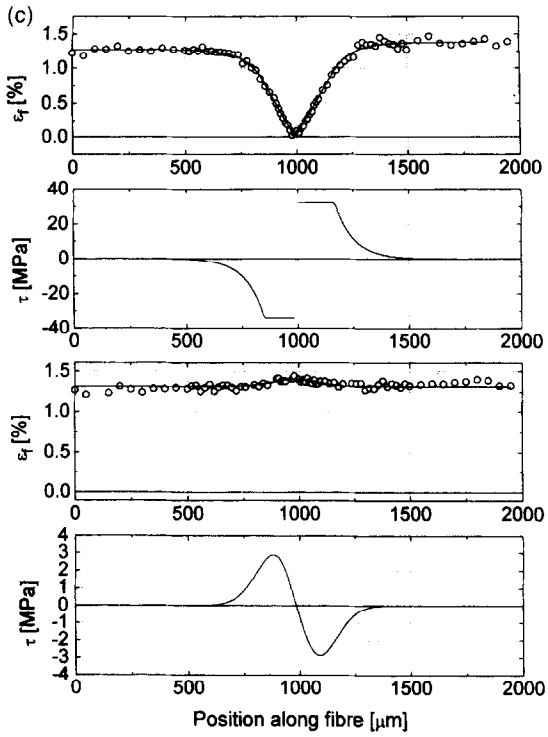

Fig. 8. (*Continued.*)

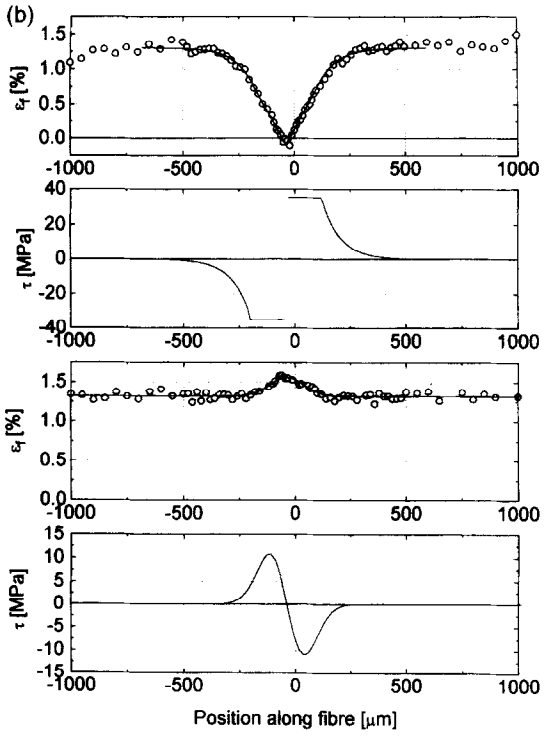

Fig. 8. Fitted strain profiles and the associated interfacial shear stresses for both the broken fibre and an adjacent fibre at (a) a relatively small inter-fibre spacing of 0·8 fibre diameters, (b) an intermediate inter-fibre spacing of 2·4 fibre diameters, (c) a relatively large inter-fibre spacing of 10·4 fibre diameters.

associated interfacial shear stresses are calculated using eqn (9) and are plotted as well.

3.4 SCF and shear stress versus inter-fibre spacing

For a variety of inter-fibre spacings the fitting procedure described above was used to determine the maximum SCF. This was undertaken for breaks which met the following two criteria only: (i) the break had to be 'isolated' from other breaks, i.e. the break under consideration was sufficiently far away from other fibre breaks in the sample; (ii) fibre/matrix debonding was absent (virtually). As observed experimentally[31] and predicted by other researchers[11,12,32] debonding alters the stress state around a fibre break and reduces the SCF significantly. The results are listed in Table 1 and the SCF values are plotted as a function of the inter-fibre spacing in Fig. 10. In Fig. 10 the SCF as a function of inter-fibre spacing predicted by some of the SCF theories[6,8,10–12,14,15,17,18] described in Section 1 are plotted also.

Figure 11 shows the influence of the maximum ISS in the fibres adjacent to a broken fibre as a function of the inter-fibre spacing (see also Table 1). The maximum ISS in case of the 2·0ϕ inter-fibre spacing could not be determined well because of scatter in the data at the base of the overload peak. This scatter did not, however, affect the determination of the maximum SCF.

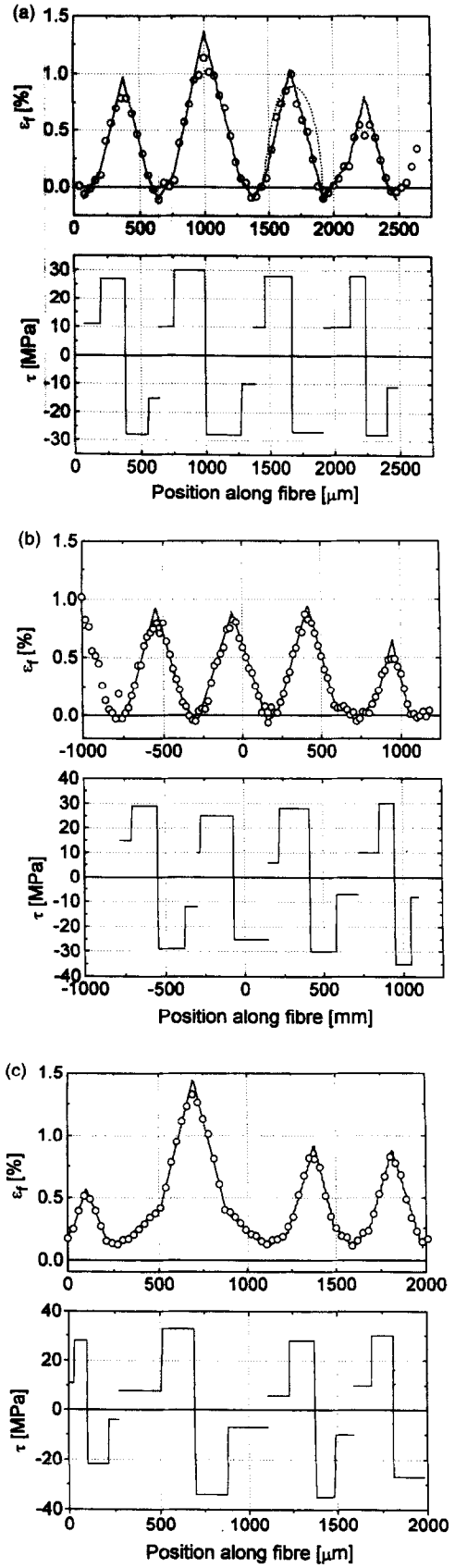

Fig. 9. Fitted strain profiles and the associated interfacial shear stresses for a fibre after saturation of the fragmentation process using eqns (10) and (9), respectively. (a) Fibre 4 of Fig. 5(d), (b) Fibre 5 of Fig. 6(c), (c) Fibre 4 of Fig. 7(c). In (a) a strain profile according to eqn (7) is also plotted (···).

4 DISCUSSION

4.1 Stress build-up in the fibres

As shown in Figs 5–7, in each microcomposite all fibres are initially under the same strain. In general, in the unstressed samples the fibres are subjected to a compressive strain of −0·1 to −0·3%. This can probably be explained by the difference in thermal expansion coefficient between the fibre and the matrix resulting in thermal residual stresses after curing the sample.[19] Occasionally, however, the fibres in the unstrained microcomposite were observed to be in tension as, for instance, shown in Fig. 7(a). This can probably be explained by a higher pre-load in the fibres in the alignment stage of the sample preparation.[25]

On increasing strain until initial fibre failure occurs, the resulting strain profiles contain a wealth of information about the mechanism of stress build-up in each of the fibres. From Figs 5(b), 6(b) and 7(b) and more particularly from Fig. 8 it is observed that the ineffective length, i.e. the length over which the stress builds up from zero at the fibre break to the applied stress, is approximately 500 μm at an applied strain of about 1·2%. This length agrees well with the length over which birefringence in the matrix is observed

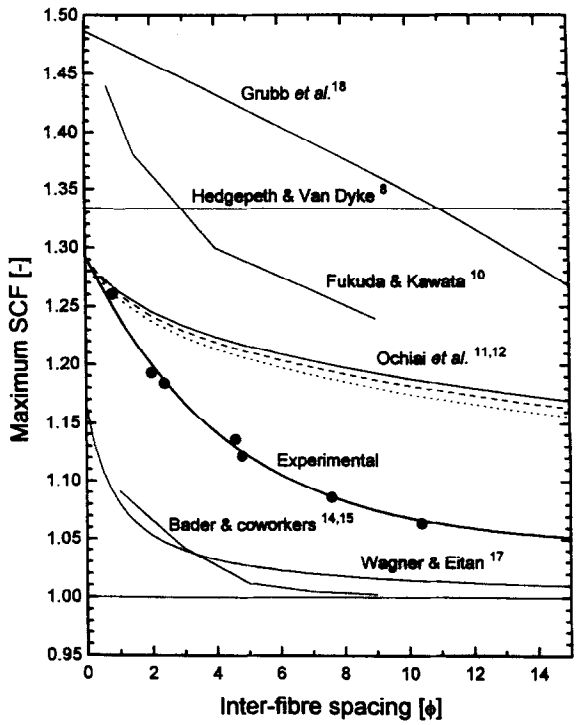

Fig. 10. Comparison of the experimentally determined variation of the maximum SCF with inter-fibre spacing with theoretical predictions. For the results of Ochiai *et al.*[11,12] three curves are plotted for $E_m = 2{\cdot}7$ GPa and various E_f values: ———, $E_f = 400$ GPa; – – –, $E_f = 350$ GPa; ···, $E_f = 300$ GPa.

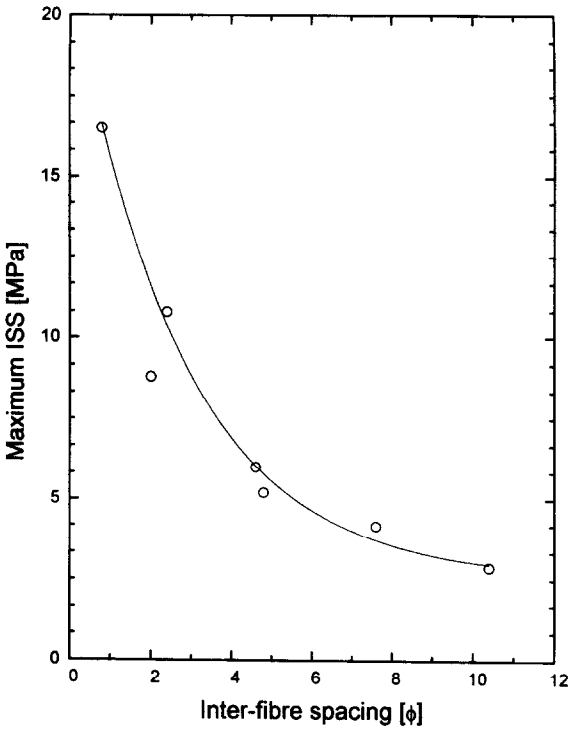

Fig. 11. Variation of the maximum interfacial shear stress with inter-fibre spacing at the fibre adjacent to a break.

using a polarized-light microscope (Fig. 12). Similar observations were reported by Grubb *et al.*[18] In Fig. 12 it can also be seen that matrix cracking and fibre/matrix debonding are absent. In the present context, the absence of matrix cracking is equally important as the absence of fibre/matrix debonding since matrix cracking is found to increase the SCF[13,18] whereas debonding is found to reduce the SCF.[11,12,31,32] Further, Fig. 8 clearly shows that over approximately the first 140–160 μm of the ineffective length, linear stress build-up takes place with an interfacial shear stress of around 30 MPa. This shear stress is a little less than the shear yield stress of the neat matrix (37 MPa) and, hence, it is concluded that local yielding of the interface takes place immediately behind the fibre break, which is in agreement with Van den Heuvel *et al.*[33] and Gulino *et al.*[34] In a

Table 1. Experimentally determined maximum SCFs and maximum ISSs at the fibres adjacent to a break at different inter-fibre spacings

Inter-fibre spacing (ϕ)	Maximum SCF	τ_{max} (MPa)
0·8	1·26	17
2·0	1·19	9
2·4	1·18	11
4·6	1·14	6
4·8	1·12	5
7·6	1·09	4
10·4	1·06	3

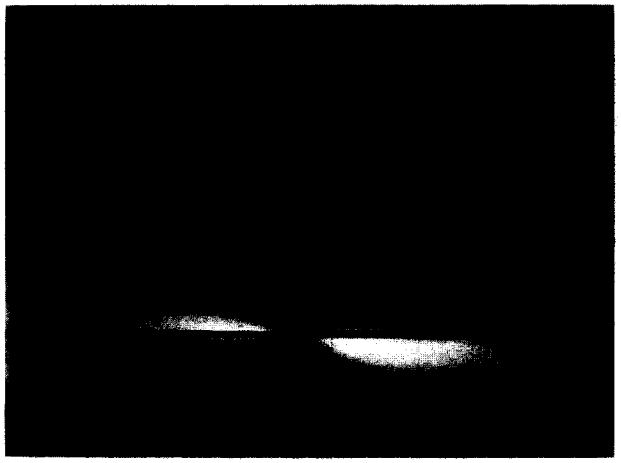

Fig. 12. Polarized-light micrograph of a 2-D Tenax HMS-40/epoxy microcomposite with a relatively large inter-fibre spacing, showing the birefringence in the matrix around a fibre break.

forthcoming paper experimental data will be presented showing that this local yielding limits the stress transfer from the matrix to the fibre.[35]

Returning to the positively affected length (Fig. 1), it is found that this length mirrors the ineffective length. The strain profile along the positively affected length is symmetrical and its maximum is situated directly adjacent to the fibre break (Fig. 8). Similar observations were reported by Grubb *et al.*[18] in their hybrid microcomposites.

4.2 SCF and its influence on the failure process

Figure 10 shows the influence of the inter-fibre distance on the maximum SCF. It can be seen that the maximum SCF decreases exponentially from a value of 1·26 at an inter-fibre spacing of 0·8ϕ to a value of 1·06 at an inter-fibre spacing of 10·4ϕ (Table 1). The curve levels off at unity far away from the fibre break, i.e. the stress situation in a fibre sufficiently far away from a fibre break is not influenced by this break. This trend is in agreement with the well-known stress distribution at a crack-tip in a solid material.[36] Figure 11 shows the maximum interfacial shear stress causing the SCF in an adjacent fibre as a function of the inter-fibre distance. It can be seen that the maximum ISS decreases in a similar way to the SCF with increasing inter-fibre spacing. At an inter-fibre spacing of 0·8ϕ the maximum interfacial shear stress is approximately 16 MPa, decreasing to a value of approximately 3 MPa at an inter-fibre distance of 10·4ϕ.

Comparing the experimental SCFs with the theoretical predictions plotted in Fig. 10, it is shown that the theory of Hedgepeth and Van Dyke[8] does not agree with the experimental results. Their SCF prediction ($K = 1{\cdot}33$) is too high, especially at intermediate and large inter-fibre spacings. Ochiai *et al.*[11,12] on the other hand, are able to predict the SCF

fairly well at an inter-fibre spacing of around 1ϕ. In addition, the shape of the predicted curve is good, although at intermediate and large inter-fibre spacings too high SCFs are predicted. Figure 10 also shows the influence of the ratio E_f/E_m on the SCF predicted by Ochiai *et al.*[11,12] It is observed that a decrease of the ratio E_f/E_m results in a decrease of the SCF. An unrealistically low E_f/E_m is, however, needed to fit the experimental data. Fukuda and Kawata[10] also predict SCFs that are too high, but the trend, i.e. shape, of the predicted curves is similar to the one found experimentally. Bader and coworkers[14,15] and Wagner and Eitan[17] predict a trend similar to that found experimentally as well, but their SCFs are too low. For plotting the theory of Grubb *et al.*[18] a fibre/fibre interaction radius, r_e, of 12ϕ was assumed based on our experimental observations. Figure 10 shows that the dependence of the SCF on the inter-fibre spacing predicted by Grubb *et al.*[18] does not fit the experimental results, and worse still, it does not predict the trend correctly.

One reason for the disagreement between all these theories and the experimental data is that all these theories are based on elastic stress transfer and, therefore, do not take into account the experimentally observed local yielding at the interface near the fibre break. In a recent paper, Ochiai *et al.*[13] show that such local yielding decreases the SCF in the adjacent fibres and it may very well be that this theory is in better agreement with the experimental results. Presently, we are implementing this theory and we hope to report on the results in the near future.

The Raman experiments also provide information about the effect of the SCF on the failure process in the microcomposite. At a small inter-fibre spacing the large SCF present in the adjacent fibres initiate fibre fracture, as can be seen in Fig. 5(c). This so-called interacted fibre failure results in alignment of the fibre breaks and ultimately results in a band-like structure at the saturation stage, as reported previously.[24,25,37] After saturation of the fragmentation process some debonding at the fibre-ends has occurred. From Fig. 9(a) it can be determined that the frictional shear stress in the debonded regions is approximately 10 MPa. In the well-bonded regions linear stress transfer through the yielded matrix at the interface continuous to take place with a shear stress of approximately 30 MPa.

The SCFs at intermediate inter-fibre spacings are much lower and, consequently, there is less coordinated fibre failure. For instance, the strain concentrations in Fibres 2 and 4 resulting from the initial fibre break at $x = 0\,\mu$m in Fig. 6(b) do not result in fibre breaks in Fig. 6(c). Apparently, other fibre breaks occurring during the increase in strain resulted in more dominant strain concentrations. Some alignment of fibre breaks can, however, be observed around $x = -750\mu$m, $x = -250\mu$m, and $x = 1100\mu$m.

At a large inter-fibre spacing the SCFs are very small and, hence, the occurrence of coordinated fibre failure is little. In Part 1 of this series of papers[25] it was found that at inter-fibre spacings smaller than 9ϕ a transition from coordinated fibre failure to random fibre failure occurs, which was also reported by Jones and DiBenedetto.[37] From Fig. 10 it can be determined that at this inter-fibre spacing the SCF is approximately 1·07. Indeed, in Fig. 7(c) it can be seen that between Fibres 2 and 3 and between Fibres 4 and 5 (both at an inter-fibre spacing of approximately 10ϕ) some coordinated fibre failure has occurred, whereas more or less random failure has occurred between the other fibres, which are at a larger inter-fibre spacing. It is also found that compared to the small and intermediate inter-fibre spacings more debonding has occurred at the saturation stage in the case of large inter-fibre spacing (Fig. 9). This could be just an artefact of the particular sample investigated, but it could also be the result of the lower SCF present at the large inter-fibre spacing. Since, when after initial fibre failure the strain is increased further, the SCF is too low to cause immediate fibre failure and relatively high macroscopic strains are needed to cause further fragmentation. Now, whenever fibre breaks do occur at these higher strains, there is much more strain energy to be released and, hence, the debonded length is expected to be larger.[33,38]

Of course, linking the experimental results with the macroscopic mechanical properties of unidirectional (UD) carbon reinforced composites is our ultimate objective. The results presented here indicate that in a real unidirectional fibre-reinforced composite of the same carbon/epoxy combination, where very small inter-fibre spacings are present, alignment of fibre breaks can be expected together with very little debonding around those breaks. In other words, brittle fracture is expected. With respect to the SCF in a UD fibre-reinforced composite, several theories reported in the literature predict a lower SCF.[8,32] In a UD composite, the excess stress caused by a fibre failure is distributed among many more neighbouring fibres. Hence, the SCF will be lower. Both these issues are under current investigation and we hope to report on this in the near future.

5 CONCLUSIONS

It has been shown that Raman spectroscopy is a very useful technique not only for determining stress concentration factors resulting from fibre breaks in a 2-D array of carbon fibres embedded in an epoxy microcomposite, but also for investigating the effect of the SCF on the subsequent failure process. For a series of microcomposites having inter-fibre spacings ranging from $0{\cdot}8\phi$–$19{\cdot}0\phi$ the SCF was measured and found to decrease from a value of 1·26 at an inter-fibre spacing of $0{\cdot}8\phi$ to a value of 1·06 at an

inter-fibre spacing of 10·4ϕ. At higher inter-fibre spacings no significant SCF could be determined. The variation of SCF with inter-fibre spacing found experimentally was compared to various theoretical predictions available in the literature. It was found that none of the theories was able to describe the experimental data adequately. Some theories predicted SCFs much higher than those found experimentally, whereas others predict SCFs much lower than found experimentally. Improvements of the various theories can probably be made by incorporating local yielding of the interface in the vicinity of the fibre break, which is observed in the strain profiles along the broken fibres. Promising results have been obtained in a preliminary finite element study incorporating such local yielding. We hope to report on these finite element results in a forthcoming paper. The influence of the inter-fibre spacing on the interfacial shear stress at the fibre adjacent to a break was determined as well. A decrease of interfacial shear stress with increasing inter-fibre spacing was found.

Furthermore, the effect of the SCF on the failure process was discussed. It was found that at relatively small inter-fibre spacings the SCF is sufficiently high to cause fibre failure. So-called coordinated fibre failure takes place resulting in the alignment of fibre breaks. At increasing inter-fibre spacing the decrease in SCF results in a decreasing influence of the initial fibre break on the subsequent failure process, i.e. the failure process becomes more random.

ACKNOWLEDGEMENTS

The authors would like to thank Huntsman NV Belgium for supplying the Jeffamine T-403 curing agent, Ciba Geigy (Duxford, UK) for supplying the Araldite LY556 resin and Akzo Fibers GmbH and Co. KG for supplying the carbon fibres. One of the authors (R.J.Y.) is grateful to the Royal Society for support in the form of the Wolfson Research Professorship in Materials Science. This work was supported in part by a grant from the EPSRC.

REFERENCES

1. Johnson, J. W. and Thorne, D. J., Effect of internal polymer flaws on strength of carbon fibres prepared from an acrylic precursor. *Carbon*, 1969, **7,** 659.
2. Hitchon, J. W. and Phillips, D. C., The dependence of the strength of carbon fibres on length. *Fibre Sci. Technol.*, 1979, **12,** 217.
3. Asloun, El. M., Donnet, J. B., Guilpain, G., Nardin, M. and Schultz, J., On the estimation of the tensile strength of carbon fibres at short lengths. *J. Mater. Sci.*, 1989, **24,** 3504.
4. Daniels, H. E., The statistical theory of the strength of bundles of threads. *Proc. R. Soc. Lond.*, 1945, **183A,** 405.
5. Rosen, B. W., Tensile failure of fibrous composites. *AIAA J.*, 1964, **2,** 1985.
6. Wolstenholme, L. C., A dependent bundles model for estimating stress concentrations in fibre-matrix composites. *J. Mater. Sci.*, 1991, **26,** 4599.
7. Harlow, D. G. and Phoenix, S. L., The chain-of-bundles probability model for the strength of fibrous materials I: Analysis and conjectures. *J. Comp. Mater.*, 1978, **12,** 195.
8. Hedgepeth, J. M. and Van Dyke, P., Local stress concentrations in imperfect filamentary composite materials. *J. Comp. Mater.*, 1967, **1,** 294.
9. Cox, H. L., The elasticity and strength of paper and other fibrous materials. *Br. J. Appl. Phys.*, 1952, **3,** 72.
10. Fukuda, H. and Kawata, K., On the stress concentration factor in fibrous composites. *Fibre Sci. Technol.*, 1976, **9,** 189.
11. Ochiai, S., Schulte, K. and Peters, P. W. M., Strain concentration factors for fibers and matrix in unidirectional composites. *Comp. Sci. Technol.*, 1991, **41,** 237.
12. Ochiai, S., Hojo, M. and Osamura, K., General expression of the shear lag analysis for unidirectional elastic fiber-elastic matrix composites. *Zeitschrift für Metallkunde*, 1993, **84,** 796.
13. Ochiai, S. and Hojo, M., Stress disturbances arising from cut fiber and matrix in unidirectional metal matrix composites calculated by means of a modified shear lag analysis. *J. Mater. Sci.*, in press.
14. Bader, M. G., Smith, R. L. and Pitkethly, M. J., Probabilistic models for hybrid composites. In *Proc. 6th Int. Conf. on Composite Materials (ICCM-6), and 2nd Eur. Conf. on Composite Materials (ECCM-2)*, Vol. 5, ed. F. L. Matthews, N. C. R. Buskell, J. M. Hodgkinson and J. Morton. Elsevier Applied Science, London, 1987, p. 481.
15. Clarke, D. A. and Bader, M. G., The influence of a polymer matrix and polymer coatings on the strength of silicon carbide reinforcing fibres. In *Proc. 6th Int. Conf. on Composite Materials (ICCM-6), and 2nd Eur. Conf. on Composite Materials (ECCM-2)*, Vol. 5, ed. F. L. Matthews, N. C. R. Buskell, J. M. Hodgkinson and J. Morton. Elsevier Applied Science, London, 1987, p. 382.
16. Cherepanov, G. P., *Mechanics of Brittle Fracture*. McGraw-Hill International, New York, 1979, pp. 616–731.
17. Wagner, H. D. and Eitan, A., Stress concentration factors in two-dimensional composites: effects of material and geometrical parameters. *Comp. Sci. Technol.*, 1993, **46,** 353.
18. Grubb, D. T., Li, Z.-F. and Phoenix, S. L., Measurement of stress concentration in a fiber adjacent to a fiber break in a model composite. *Comp. Sci. Technol.*, 1995, **54,** 237.
19. Huang, Y. and Young, R. J., Interfacial behaviour in high temperature cured carbon fibre/epoxy resin model composite. *Composites*, 1995, **26,** 541.
20. Gu, X. H., Young, R. J. and Day, R. J., Deformation micromechanics in model carbon fibre-reinforced composites: 1. The single-fibre pull-out test. *J. Mater. Sci.*, 1995, **30,** 1409.
21. Vlattas, C. and Galiotis, C., Deformation behaviour of liquid crystal polymer fibers: I. Converting spectroscopic data into mechanical stress–strain curves in tension and compression. *Polymer*, 1994, **35,** 2335.
22. Wagner, H. D., Amer, M. S. and Schadler, L. S., Fibre interactions in two-dimensional composites by micro-Raman microscopy. *J. Mater. Sci.*, 1996, **31,** 1165.
23. Van den Heuvel, P. W. J., Peijs, T. and Young, R. J.,

Analysis of stress concentrations in multi-fibre microcomposites by means of Raman spectroscopy. *J. Mater. Sci. Lett.*, 1996, **5**, 1908.
24. Van den Heuvel, P. W. J., Van der Bruggen, Y. J. W. and Peijs, T., The influence of carbon fibre surface treatment on fibre–fibre interactions in multi-fibre microcomposites. *Adv. Comp. Lett.*, 1994, **3**, 197.
25. Van den Heuvel, P. W. J., Van der Bruggen, Y. J. W. and Peijs, T., Failure phenomena in multi-fibre model composites: 1. An experimental investigation into the influence of fibre spacing and fibre-matrix adhesion. *Composites A*, 1996, **27A**, 855.
26. Drzal, L. T., Rich, M. J., Koenig, M. F. and Lloyd, P. F., Adhesion of graphite fibers to epoxy matrices: II. The effect of fiber finish. *J. Adhesion*, 1983, **16**, 133.
27. Piggott, M. R., Expressions governing stress–strain curves in short fibre reinforced polymers. *J. Mater. Sci.*, 1978, **13**, 1709.
28. Lacroix, Th., Tilmans, B., Keunings, R., Desaeger, M. and Verpoest, I., Modelling of critical fibre length and interfacial debonding in the fragmentation testing of polymer composites. *Comp. Sci. Technol.*, 1992, **43**, 379.
29. Galiotis, C., Interfacial studies on model composites by laser Raman spectroscopy. *Comp. Sci. Technol.*, 1991, **42**, 125.
30. Kelly, A. and Tyson, W. R., Tensile properties of fibre-reinforced metals: Copper/tungsten and copper/molybdenum. *J. Mech. Phys. Solids*, 1965, **13**, 329.
31. Van den Heuvel, P. W. J., Peijs, T. and Young, R. J., Failure phenomena in two-dimensional multi-fibre microcomposites: 3. A Raman spectroscopic study into the influence of interfacial debonding on stress concentrations. *Comp. Sci. Technol.*, submitted.
32. Nedele, M. R. and Wisnom, M. R., Stress concentration factors around a broken fibre in a unidirectional carbon fibre-reinforced epoxy. *Composites*, 1994, **25**, 549.
33. Van den Heuvel, P. W. J., Hogeweg, B. and Peijs, T., An experimental and numerical investigation into the single fibre fragmentation test: Stress transfer by a locally yielding matrix. *Composites A*, 1997, **28**, 237.
34. Gulino, R., Schwartz, P. and Phoenix, S. L., Experiments on shear deformation, debonding and local load transfer in a model graphite/glass/epoxy microcomposite. *J. Mater. Sci.*, 1991, **26**, 6655.
35. Van den Heuvel, P. W. J., Peijs, T. and Young, R. J., in preparation.
36. Westergaard, H. M., Bearing pressures and cracks. *J. Appl. Mech.*, 1939, **6**, A49.
37. Jones, K. D. and DiBenedetto, A. T., Fiber fracture in hybrid composite systems. *Comp. Sci. Technol.*, 1994, **51**, 53.
38. Wagner, H. D. and Ling, S., An energy-based interpretation of interfacial adhesion from single fibre composite fragmentation testing. *Adv. Comp. Lett.*, 1993, **2**, 169.